



1 **A Time-Dependent Three-Dimensional Magnetopause Model** 2 **Based on Quasi-elastodynamic Theory**

3 Yaxin Gu^{1,2}, Yi Wang^{1*}, Fengsi Wei¹, Xueshang Feng¹, Andrey Samsonov², Xiaojian Song³, Boyi
4 Wang¹, Pingbing Zuo¹, Chaowei Jiang¹, Yalan Chen¹, Xiaojun Xu⁴, Zilu Zhou⁴

5 1 Shenzhen Key Laboratory of Numerical Prediction for Space Storm, College of Aerospace Science and
6 Technology, Harbin Institute of Technology, Shenzhen, 518055, China

7 2 Mullard Space Science Laboratory, University College London, Dorking, RH56NT, United Kingdom

8 3 Shandong High Technology Research, Shandong, 250100, China

9 4 State Key Laboratory of Lunar and Planetary Sciences, Macau University of Science and Technology, Macau,
10 999078, China

11 *Correspondence to: Yi Wang (wingwy@mail.ustc.edu.cn)

12 **Abstract.** The interaction between the solar wind and Earth's magnetosphere is a critical area of
13 research in space weather and space physics. Accurate determination of the magnetopause position is
14 essential for understanding magnetospheric dynamics. While numerous magnetopause models have
15 been developed over past decades, most are time-independent, limiting their ability to elucidate the
16 dynamic movement of the magnetopause under varying solar wind conditions. This study introduces
17 the first time-dependent three-dimensional magnetopause model based on quasi-elastodynamic theory,
18 named the POS (Position-Oscillation-Surface wave) model. Unlike existing time-independent models,
19 the POS model physically reflects the dynamic responses of magnetopause position and shape to time-
20 varying solar wind conditions. The predictive accuracy of the POS model was evaluated by using
21 38,887 observed magnetopause crossing events. The model achieved a root-mean-square error of 0.768
22 Earth radii (R_E), representing a 18.7% improvement over five widely used magnetopause models.
23 Notably, the POS model demonstrated superior accuracy under highly disturbed solar wind conditions
24 (24.9% better) and in higher latitude regions (28.7% better) and flank regions (35.2% better) of the
25 magnetopause. The POS model's remarkable accuracy, concise formulation, and fast computational
26 speed enhance our ability to predict magnetopause position and shape in real-time. This advancement
27 is significant for understanding the physical mechanisms of space weather phenomena and improving



28 the accuracy of space weather forecasts. Furthermore, this model may provide new insights and
29 methodologies for constructing magnetopause models for other planets.

30 **1 Introduction**

31 The magnetopause, the boundary between the interplanetary magnetic field (IMF) and Earth's
32 magnetic field, plays a crucial role in space weather forecasting and understanding solar wind-
33 magnetosphere coupling mechanisms (Willis, 1971; P. Song, 1996; Russell, 2003). It acts as a
34 protective shield against hazardous energetic particles while simultaneously serving as the primary
35 interaction region for solar wind-magnetosphere coupling. The magnetopause exhibits considerable
36 dynamic behaviour due to continuous solar wind variations and various instabilities, even under steady
37 solar wind conditions (Anderson et al., 1968; Song et al., 1988; Eastwood et al., 2015). These dynamics
38 can lead to radiation belt particle loss, field-aligned current intensification, ultra-low frequency wave
39 generation, and solar wind energy conversion into the radiation belts, polar regions, and ionosphere
40 (Haerendel, 1990; Mann et al., 2012; Plaschke, 2016; Mottez, 2016; Archer et al., 2019). Consequently,
41 comprehending the interactions between solar wind and magnetopause is vital for advancing
42 magnetosphere dynamics and improving space weather prediction capabilities (Feng, 2020; Zong et
43 al., 2020).

44 Numerous magnetopause models have been established over the past few decades, generally
45 categorized as physical (or principal) models (Ferraro, 1952; Beard, 1960; Spreiter et al., 1966) and
46 empirical models (Fairfield, 1971; Tsyganenko, 1989; Shue et al., 1998; Lin et al., 2010). Physical
47 models are primarily based on the classic Chapman-Ferraro theory proposed in the 1930s (Chapman
48 and Ferraro, 1930), which states that the magnetopause's equilibrium position is determined by the
49 pressure balance between solar wind dynamic pressure (P_{dyn}) and magnetospheric magnetic pressure
50 (P_b). Since the 1960s, the launch of numerous satellites has provided us with a large number of samples
51 of magnetopause crossing events (MCEs), thereby creating the possibility for the establishment of
52 empirical models (Fairfield, 1971; Sibeck, 1991; Petrinec and Russell, 1996; Shue et al., 1998; Lin et



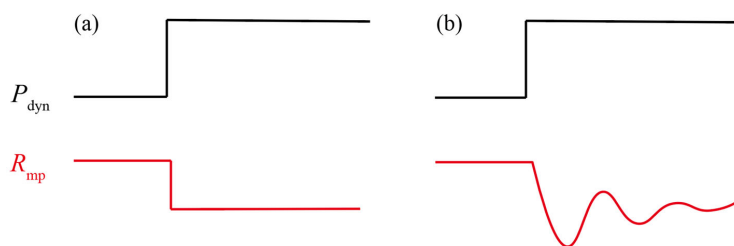
53 al., 2010). Many empirical models rely on two key parameters, P_{dyn} and IMF B_z , and some of them
54 include the Earth's dipole tilt angle (Φ) to calibrate the higher latitude zone. Besides, some empirical
55 models, proposed from the 1980s, combine physical processes of solar wind-magnetosphere
56 interactions with satellite observation fitting and involved the impact of magnetospheric currents
57 system (Tsyganenko, 1989, 1996). Regardless of the assumptions on which these models are based,
58 all these models have contributed to our understanding of magnetopause movement and its response
59 to solar wind conditions, in particular, many of them have been widely used in the prediction of the
60 magnetopause due to their simple form and high prediction accuracy.

61 However, it should be aware that these models primarily describe the average steady-state
62 characteristics of the magnetosphere. To accurately describe the dynamic coupling process of solar
63 wind-magnetosphere interaction, it is essential to incorporate time partial derivatives into the dynamic
64 equations (Smit, 1968; Petrinec, 2001; Borovsky and Alejandro Valdivia, 2018). This approach,
65 however, complicates the solution of model equations, often necessitating numerical simulations such
66 as magnetohydrodynamics (MHD) (Powell et al., 1999; Raeder et al., 2001; Lyon et al., 2004; Tóth et
67 al., 2005; Merkin and Lyon, 2010), particle-in-cell (PIC) (Moritaka et al., 2012; Ashida et al., 2014;
68 Walker et al., 2019), and hybrid simulations (Gargaté et al., 2008; Omelchenko et al., 2021; Ala-Lahti
69 et al., 2022). Numerical simulations are widely used in exploring solar wind-magnetosphere coupling
70 and can accurately reveal the position of the magnetopause changing with the time-varying solar wind.
71 Their prediction accuracy is generally much better than the magnetopause model mentioned above.
72 However, the introduction of time partial derivatives makes equations very difficult to solve. In
73 addition, many prominent numerical simulation models may not include properly all magnetospheric
74 current systems (e.g. the ring current or the magnetospheric-ionospheric currents), therefore this may
75 result in systematic errors of the magnetopause prediction (Samsonov et al., 2016). Moreover,
76 numerical models are solved on supercomputers, consuming a significant amount of computing
77 resources and time, rendering them impractical for real-time space weather forecasting (Raeder et al.,
78 2001; Lyon et al., 2004; Tóth et al., 2005; Feng, 2020). This limitation highlights the need for more



79 efficient, yet accurate, magnetopause models that can capture the dynamic nature of the magnetopause
80 while remaining computationally feasible for real-time applications. Such models would significantly
81 enhance our ability to predict and understand space weather phenomena, bridging the gap between
82 theoretical understanding and practical forecasting capabilities.

83 Apart from numerical simulations, very few time-dependent magnetopause models have been
84 historically developed (Smit, 1968; Freeman et al., 1995; Børve et al., 2011). Figure 1 illustrates the
85 fundamental difference between time-independent and time-dependent models. In time-independent
86 models, the magnetopause position is directly correlated with instantaneous solar wind conditions. For
87 example, a step-like increase in solar wind dynamic pressure (such as a shock) corresponds to an
88 immediate step-like compression of the magnetopause (Figure 1a). However, this simplification fails
89 to capture the real dynamics of the magnetopause. In reality, the magnetopause undergoes a more
90 complex process of compression and recovery, exhibiting oscillatory characteristics in response to
91 abrupt changes in solar wind conditions, as shown in Figure 1b (Freeman and Farrugia, 1998; Hu et
92 al., 2005; Desai et al., 2021). Time-dependent models aim to capture these dynamic processes,
93 providing a more accurate representation of magnetopause behaviour. To describe these dynamic
94 responses, it is necessary to incorporate time partial derivatives into the governing equations. However,
95 this inclusion significantly complicates the solution process. Consequently, existing time-dependent
96 models are predominantly one-dimensional and remain in a preliminary stage of development.



97

98 **Figure 1 The schematic diagram of time-independent (a) and time-dependent (b) magnetopause models.**



99 Smit (1968) conceptualized the magnetopause as a rigid surface and attempted to explain its
100 motion from the perspective of periodic vibration; Freeman et al. (1995) investigated the influence of
101 inertial and damping effect on the magnetosphere, employing magnetohydrodynamics to analyse the
102 magnetopause motion; Børve et al. (2011) set up a non-adjustable model to analyse the oscillation
103 period of the magnetopause. By investigating the movement of the subsolar point in response to time-
104 varying solar wind, these models are primarily constructed to elucidate specific physical phenomena
105 linked to solar wind-magnetosphere interaction, yet they lack the capability to provide a real-time
106 depiction of the three-dimensional magnetopause position and shape.

107 Hence, the challenge of constructing time-dependent models lies in balancing the need for
108 accurate dynamic representation with computational feasibility. Although time-dependent models
109 offer a more realistic depiction of magnetopause behaviour, their complexity has limited their
110 development and application, particularly in three-dimensional space. This highlights the necessity for
111 new strategies that can capture time-dependent dynamics while ensuring practical utility for
112 computation, especially for real-time space weather forecasting and related magnetospheric researches.
113 Previously, our work revealed the quasi-elastodynamic processes involved in the interaction between
114 solar wind and magnetosphere (Gu et al., 2023). It suggests that the dynamic behaviour of each point
115 on the magnetopause can be viewed as an equilibrium position (P), radial global oscillations around
116 equilibrium position (O), and surface wave-like structure around the flank regions (S). This work offers
117 a practical framework for developing a time-dependent three-dimensional magnetopause model.

118 However, our previous work primarily focused on elucidating the quasi-elastic process, with less
119 emphasis on the outcomes of model predictions (Gu et al., 2023). Key factors influencing
120 magnetopause dynamics, such as the IMF B_z and Earth's dipole tilt angle (Φ), were not incorporated.
121 Additionally, the adjustable parameters in the equations were simply chosen and lack of thorough
122 calibrations. Moreover, both our prior work and most published magnetopause models (Petrinec and
123 Russell, 1996; Shue et al., 1998; Gu et al., 2023) relied on a relatively limited dataset of low-latitude
124 satellite observations, leading to constraints in accurately representing the higher latitude and flank



125 regions of the magnetopause. To address these limitations and overcome the inherent shortcomings of
126 time-independent models, particularly their inability to reflect the dynamic responses of the
127 magnetopause position and shape to time-varying solar wind conditions, we propose a time-dependent
128 three-dimensional magnetopause model. This model, which has been tested with the largest dataset of
129 MCEs to date (38,887 events), demonstrates remarkable prediction accuracy compared to five widely
130 used magnetopause models. Besides, it offers unparalleled real-time computation speed and a concise
131 form relative to numerical simulations. We have named this model the Position-Oscillation-Surface
132 wave (POS) model.

133 **2 Dataset and other magnetopause models for comparison**

134 The THEMIS (Time History of Events and Macroscale Interactions during Substorms) mission
135 (Angelopoulos, 2008), which consists of five spacecrafts launched into similar elliptical, near-
136 equatorial orbits in 2007, has significantly enhanced our ability to observe the magnetosphere. The
137 mission provides high-resolution (~3 s) magnetic field measurements through the THEMIS/Flux Gate
138 Magnetometer (FGM) (Auster et al., 2008) and plasma data from the THEMIS/electrostatic analyser
139 (ESA) (Mcfadden et al., 2008). The Cluster II mission (Escoubet et al., 2001), involving four identical
140 spacecraft launched in 2000, also offers high-resolution (~4 s) magnetic field measurements using the
141 CLUSTER/Flux Gate Magnetometer (FGM) (Balogh et al., 1997) and particle data and moments from
142 the Cluster Ion Spectrometry Hot Ion Analyser (CIS-HIA) (RÈme et al., 1997).

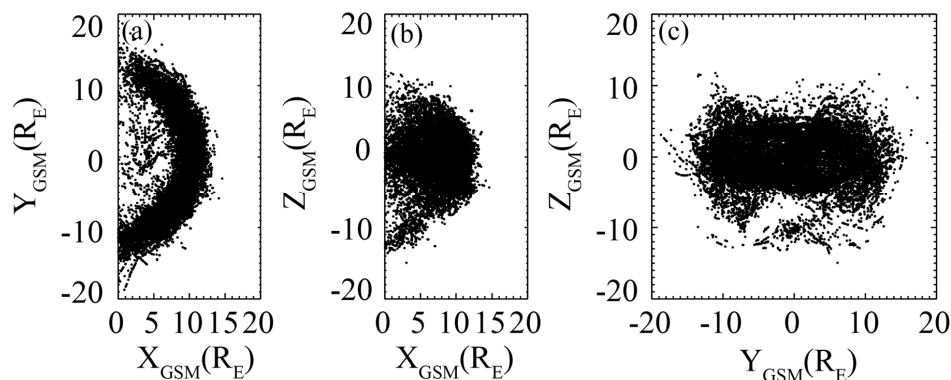
143 The WIND spacecraft, launched into orbit around Earth in 1994 and relocated to Lagrange L1
144 point after 2004, provides reliable, high-quality in situ measurements of the solar wind. This study
145 utilizes high-resolution (~3 s) plasma data from the WIND/3D Plasma Analyzer (3DP) (Lin et al.,
146 1995) and magnetic field data from the Magnetic Field Investigation (MFI) (Lepping et al., 1995) for
147 upstream solar wind observations. For this study, we have compiled a dataset consisting of 51,590
148 THEMIS MCEs and 38,321 Cluster MCEs. After excluding redundant, invalid data and nightside
149 MCEs ($X_{GSM} < 0 R_E$), a total of 38,018 THEMIS MCEs and 869 CLUSTER MCEs (see Figure 2) are



150 matched with upstream solar wind observations. The time shift (Δt) from WIND to each MCE was
 151 determined by comparing the time of each magnetopause crossing (t_1) with the estimated arrival time
 152 of the corresponding solar wind observation from WIND ($t_0 + \Delta t$). This condition was satisfied when
 153 $(t_0 + \Delta t) - t_1 < 300$ s, where Δt was calculated using the formula $\Delta t = (L1 - r) / \langle v_x \rangle$. Here, $\langle v_x \rangle$
 154 represents the 1-hour sliding average of the solar wind velocity's x-component as observed by WIND
 155 at L1 ($L1 = 235 R_E$), and r is the radial position of the magnetopause derived from each MCE. A
 156 summary of these events is provided in Table 1. The distribution of matched solar wind conditions for
 157 MCEs is shown in Figure 3. All the data is available in the CDAWeb database
 158 (<http://cdaweb.gsfc.nasa.gov/>), and the time resolution of the magnetic field and plasma data used in
 159 the study is interpolated into 3 seconds, set in GSM coordinates.

160 **Table 1 Summary of collected 89,911 satellite MCEs and dataset used in this paper**

Dataset	Satellite	Time interval	Number of datasets
Song et al. (2021)	THEMIS	2007-2022	17,647
Staples et al. (2020a)	THEMIS	2007-2016	33,943
Grimmich (2024)	CLUSTER	2001-2020	38,321
In this paper	THEMIS/CLUSTER	2004-2022	38,887

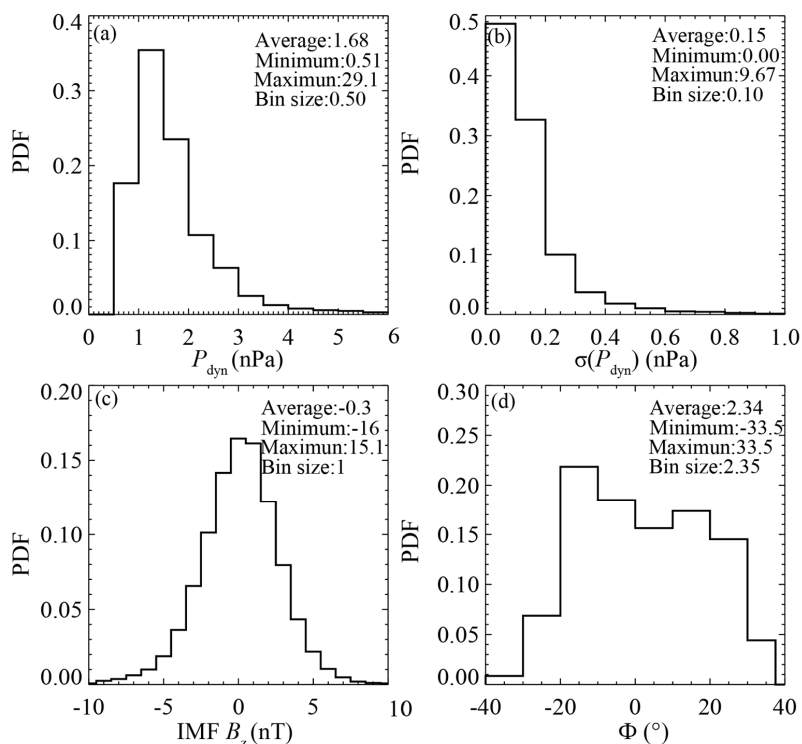


161

162 **Figure 2 Projections of 38,887 MCEs in GSM coordinate: (a) X-Y plane, (b) X-Z plane, (c) Y-Z plane.**



163 In previous research on time-independent magnetopause models, the physical models (Ferraro,
164 1952; Beard, 1960; Spreiter et al., 1966), although theoretically grounded, usually oversimplify
165 intricate solar wind-magnetosphere interactions to facilitate calculations, usually without
166 demonstrating apparent higher prediction accuracy compared to widely-used empirical models
167 (Petrinec and Russell, 1996; Shue et al., 1997; Shue et al., 1998; Chao et al., 2002; Lin et al., 2010).
168 Hence, this article concentrates on comparing several notable time-independent empirical models
169 renowned for their superior prediction accuracy (Petrinec and Russell, 1996; Shue et al., 1997; Shue
170 et al., 1998; Chao et al., 2002; Lin et al., 2010).



171

172 **Figure 3** Probability density function of the upstream solar wind observation in: (a) solar wind dynamic
173 pressure P_{dyn} , (b) standard deviation of dynamic pressure (P_{dyn}), (c) interplanetary magnetic field B_z
174 component (IMF B_z) and (d) dipole tilt angle (Φ).



175 Empirical models are typically constructed using satellite observations of MCEs. While these
176 models vary in their use of satellite datasets, parameters considered, coordinate systems employed,
177 and functions applied, most are parameterized using the dynamic pressure (P_{dyn}) and the interplanetary
178 magnetic field B_z component (IMF B_z). For example, Petrinec and Russell (1996) (hereafter PR96)
179 employed an ellipsoidal function to construct a magnetopause model, while Shue et al. (1997)
180 (hereafter S97) developed a flexible function incorporating two variables: the subsolar magnetopause
181 position (R_0) and the tail flaring angle (α). This function has gained widespread use as a foundational
182 approach to describing magnetopause shape. For instance, Shue et al. (1998) (hereafter S98) accounted
183 for the saturation effect of IMF B_z on R_0 , and Chao et al. (2002) (hereafter C02) extended their model
184 for application under normal and extreme solar wind conditions.

185 Nevertheless, these models primarily rely on low-latitude satellite observations and may not
186 adequately capture the distinctive characteristics of the magnetopause in the higher latitude region.
187 Besides, they are constructed with P_{dyn} and IMF B_z , while it is found that the dipole tilt angle Φ is of
188 great significance in modelling magnetopause, especially in the higher latitude region. Formisano et
189 al. (1979) constructed an average magnetopause size and shape for two dipole tilt angle values (Φ).
190 Boardsen et al. (2000) developed a higher latitude magnetopause model parameterized by not only
191 P_{dyn} and IMF B_z but also the dipole tilt angle (Φ), recognizing its significant influence on the shape of
192 the higher latitude magnetopause. While this model is specifically designed for higher latitude regions,
193 it is not as effective in accurately calculating the magnetopause at low latitudes compared to other
194 models due to inherent limitations.

195 The above models are generally developed under the assumption of axial symmetry, while the
196 actual magnetopause shape is asymmetric in both the Y and Z directions, so they are essentially 2D or
197 2.5D models. To describe the 3D structure of the magnetopause, Lin et al. (2010) (hereafter L10)
198 developed a three-dimensional magnetopause model parameterized by P_{dyn} , thermal pressure (P_t), IMF
199 B_z , and Φ . The coordinate systems employed in these empirical models are typically in aberrated
200 coordinates which accounts for Earth's orbital motion (Petrinec and Russell, 1996; Shue et al., 1997;



201 Shue et al., 1998; Chao et al., 2002), or the corrected coordinates which compensates for both Earth's
202 orbital motion and deviations in solar wind velocity from the Sun-Earth line (Boardsen et al., 2000;
203 Lin et al., 2010). A summary of the five widely used magnetopause models is presented in Table 2.

204 **Table 2 Summary of five widely used magnetopause models and POS model**

Model Name	Number of (higher latitude) MCEs used	Time range of MCEs used	Dimensions
PR96	1,147	1979-1980	2D/2.5D
S97	553	1978-1986	2D/2.5D
S98	553	1978-1986	2D/2.5D
C02	552	1978-1986	2D/2.5D
L10	1,226 (1,482)	1994-2008	3D
POS	31,562 (7,325)	2004-2022	3D

205 **3 The POS Model**

206 In our previous work (Gu et al., 2023), we modelled the compression-recovery process of the
207 magnetopause as a quasi-elastodynamic phenomenon. In this framework, the dynamic pressure,
208 $P_{\text{dyn}}=n_{\text{sw}}m_p v_x^2$, serves as the driving force on the system, where n_{sw} , m_p , and v_x are the number density,
209 proton mass, and the x component of the solar wind velocity in the GSM coordinates, respectively.
210 The system's restoring force is described by, $P_b=B^2/2\mu_0$, where B is the total magnetic field at
211 magnetopause and μ_0 is the vacuum permeability. After accounting for damping and non-ideal effects,
212 P_{damp} , meanwhile neglecting the complex coupling interactions, the momentum equation for the
213 magnetosheath in a unit cylinder can be represented by equation (1).

$$214 \quad M_{\text{msh}} a_{\text{msh}} = P_b - P_{\text{dyn}} - P_{\text{damp}} \quad (1)$$

215 Given that the derivation process of the foundational formula is the same as our previous work,
216 and this paper is focused on model predictions rather than physical processes, we will refrain from



217 reiterating it here. The relationship depicting the temporal evolution of the magnetopause position (r)
218 are introduced in equation (2).

$$219 \quad n_{sw} m_p r \ddot{r} = \frac{(\lambda \mathbf{B}_d(\mathbf{r}, \theta, \varphi) + \mathbf{B}_e(\mathbf{r}))^2}{2\mu_0} - n_{sw} m_p v_x^2 \cos^2 \alpha - k \Sigma_p \mathbf{B}_p^2 \dot{r} - \eta \dot{r} / r \quad (2)$$

220 Where (r, θ, φ) represents the corresponding spherical coordinates, r is the radial distance, θ is the
221 latitude angle between $[-90^\circ, 90^\circ]$ and φ is the longitude angle adjusted to $[-180^\circ, 180^\circ]$ with 0°
222 oriented towards the Sun for simplicity, \mathbf{n} is the normal direction of magnetopause (Gu et al., 2023).
223 This simplified equation enables us to capture the fundamental dynamics of the magnetopause's
224 response to solar wind fluctuations while ensuring computational efficiency. The first term on the right
225 side of equation (2) signifies the restoring force \mathbf{P}_b . Here, \mathbf{B}_d denotes the Earth's dipole field, λ is the
226 magnetospheric compressibility coefficient, and \mathbf{B}_e accounts for contributions from various
227 magnetospheric currents. The second term on the right side represents the driving force \mathbf{P}_{dyn} , where α
228 denotes the angle between the x-direction and the normal direction of the magnetopause. The third
229 term on the right side of equation (2) characterizes a position-dependent dragging effect estimated
230 from the ionosphere, while the fourth term illustrates a global non-ideal viscous effect. \mathbf{B}_p is the
231 estimated ionospheric magnetic field in the polar region, Σ_p stands for the equivalent Pederson
232 conductivity, k serves as a position-dependent mapping factor, and η represents the viscous coefficient.
233 The final two terms contribute to the damping and non-ideal effects of the system, denoted as \mathbf{P}_{damp} .
234 Equation (2) provides a foundation for developing a time-dependent magnetopause model that can
235 reflect the system's dynamic behaviour more accurately compared to conventional time-independent
236 models. We will introduce the key parameters in detail in the following sections. All the parameters
237 are in SI units.

238 In this study, we incorporate the impact of IMF \mathbf{B}_z and Φ in the magnetospheric magnetic
239 pressure. To determine the equation's final fitting coefficients, we performed 1000 independent
240 iterations of randomly sampling 5000 MCEs sampled randomly from our dataset (a total of 38,887
241 MCEs).



242 **3.1 The magnetospheric compressibility coefficient (λ)**

243 The magnetospheric compressibility coefficient, λ , measures the magnetosphere's response to
244 solar wind pressure, specifically the ratio of the magnetospheric magnetic field to the pure dipolar
245 magnetic field (Spreiter et al., 1966; Schield, 1969). This coefficient is one of the most critical
246 parameters directly affecting the position of the magnetopause. Typically, λ has a value of 2.44 at the
247 subsolar point, but it changes as the magnetopause shifts and varies with latitude and longitude,
248 suggesting a more complex formulation (Shue et al., 2011; Chen et al., 2023). Mead and Beard (1964)
249 used a self-consistent method, discovered an inward concave structure at the higher latitude
250 magnetopause, which is influenced by the inclination angle of the Earth's dipole. Their work also
251 determined the surface shape of the magnetopause when the solar wind flow is perpendicular to the
252 dipole axis ($\Phi = 0^\circ$), providing an expression for λ as a function of the angles θ and φ .

253 Several models have been developed to examine the influence of Φ (the angle between Earth's
254 magnetic axis and the solar wind direction) on the magnetopause's position and shape, offering
255 valuable insights into the magnetosphere's three-dimensional structure (Formisano et al., 1979;
256 Boardsen et al., 2000; Lin et al., 2010). These models predict an asymmetric response of the
257 magnetosphere to variations in Φ . Boardsen et al. (2000) quantified the effects of Φ on the higher
258 latitude magnetopause using MCEs data from the northern hemisphere. Their work revealed how the
259 dipole tilt angle influences the magnetopause structure in polar regions, which are particularly sensitive
260 to changes in the orientation of Earth's magnetic field relative to the solar wind. Lin et al. (2010) further
261 demonstrated that an increase in Φ causes a slight shift in the centres of the magnetopause cross-
262 sections, moving them towards the negative Z direction in the subsolar region and towards the positive
263 Z direction in the tail region. Olson (1969) provided a more detailed representation of λ for various tilt
264 angles ($\Phi = 0^\circ, 10^\circ, 20^\circ, 30^\circ$) on a 15° by 15° grid of θ and φ values. Building from previous work (Gu
265 et al., 2023) and considering the influence of Φ on different position of magnetopause $\lambda(\theta, \varphi)$, we
266 present a more precise expression of λ tailored to our model, as shown in equation (3):



$$A = \tanh[5.568(|\theta| - 0.5325)] + 1.0$$
$$\lambda(\theta, \varphi, \Phi) = 2.44 - (0.4 + 0.3A)(\theta + 0.2A\Phi)^2 + (1.0 - 0.5A|\Phi|)\varphi^2 \quad (3)$$

3.2 Contributions from various magnetospheric currents (B_c)

Previous studies on the impact of magnetospheric currents on the position of the magnetopause led to the development of a static magnetopause current model, where the magnetic field of magnetopause surface current and tail current were fitted using polynomials to reveal the relationship between variations in the magnetospheric magnetic field and changes in magnetopause position, e.g. $B_{\text{surf}}(r, \theta, \varphi)$ and $B_{\text{tail}}(r, \theta, \varphi)$ (Choe and Beard, 1974b, a; Matsuoka et al., 1995). While our previous approach, which utilize piecewise functions, may yield discontinuous and non-physical results at the transition point (Gu et al., 2023). To address this limitation, the basic form of $B_{c0}(r, \theta, \varphi)$ in this paper is shown below:

$$B_{c0}(r) = [-401904 / (\frac{r}{R_E})^4 + 65489 / (\frac{r}{R_E})^3 + 1500 / (\frac{r}{R_E})^2 - 40][1 + 0.4 \sin(2\theta)^2][1.0 - 0.1 \sin(\varphi)] \times 10^{-9} \quad (4)$$

In addition, the influence of IMF B_z on the magnetopause position is directional dependent. A southward IMF may trigger magnetic reconnection at the dayside magnetopause, a significant effect that is incorporated in most existing models (Aubry et al., 1970; Dungey, 1961; Fairfield, 1971). In this study, we employ a hyperbolic tangent function, similar to that used in the S98 model, to better depict the impact of IMF on the magnetopause dynamics. Finally, by considering the impact of IMF B_z and P_{dyn} , and assuming that B_c would behaves differently depending on θ and φ , B_c is expressed as shown in equation (5):

$$B_c = B_{c0}(r, \theta, \varphi) f(B_z) f(P_{\text{dyn}})$$
$$= B_{c0}(r) [1.8 + \tanh(-0.3B_z + 6.14)][1 + 0.1P_{\text{dyn}}] \quad (5)$$

This formulation of B_c provides a more refined and physically accurate depiction of the influence of the magnetospheric current system on magnetopause dynamics. By incorporating the dependence of B_c on IMF B_z and P_{dyn} , and specific locations on the magnetopause, the expression captures the



289 complex spatial variations in the magnetospheric current system that contribute to magnetic pressure,
290 making our model fully three-dimensional.

291 **3.3 The damping items**

292 The damping terms, represented by the last two terms on the right side of the equation, are the
293 same as our previous work (Chen and Wolf, 1999; Wang and Chen, 2008; Gu et al., 2023). Here,
294 $B_p=3\times 10^{-5}$ T, represents the estimated ionospheric magnetic field in the polar region, and $\Sigma_p=3.4S$
295 the equivalent Pederson conductivity. The viscous coefficient is artificially set as $\eta=2\times 10^{-8}$. The
296 position-dependent mapping factor k is defined as in equation (6):

$$297 \quad k = [196(0.05 + e^{-0.05(r/R_E)^2}) - 3.2|\theta| - 1.6|\phi|] \times 10^{-7} \quad (6)$$

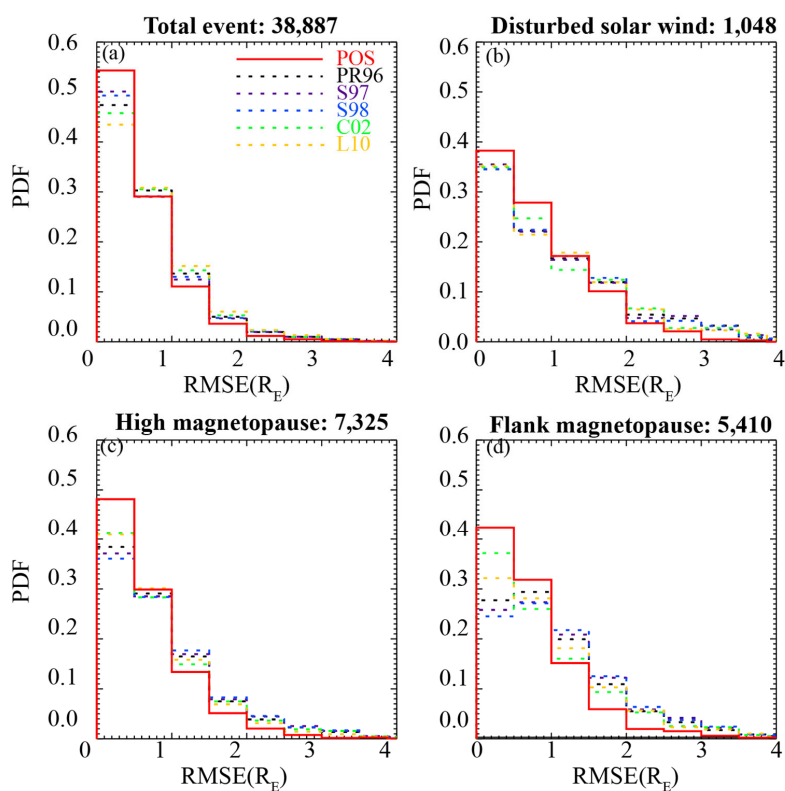
298 **4 Result**

299 By substituting the relevant parameters into equation (2) and assuming the initial shape of the
300 magnetopause as a paraboloid, $x=-0.03(y^2+z^2) + R_0$, where R_0 is determined by the pressure balance at
301 the subsolar point, the position of each point on the magnetopause can be computed instantaneously
302 on a personal computer. The prediction accuracy of the POS model is then evaluated and compared
303 with other notable time-independent models mentioned earlier. We use the root-mean-square error
304 (RMSE), denoted as Δ , to quantify the prediction accuracy by comparing the model's calculations with
305 MCEs observations. A dataset of 38,887 MCEs observed by the THEMIS and CLUSTER satellites is
306 used for testing. To evaluate the performance of the POS model relative to other models, we calculate
307 the ratio $\delta(\Delta)/\Delta_{POS}$, where $\delta(\Delta)$ represents the difference in RMSE between a previous model and the
308 POS model, and Δ_{POS} is the RMSE of the POS model. This comparison is conducted from various
309 perspectives. The probability density distributions of RMSE for each model are illustrated in Figure 4.

310 It can be seen that all models are capable of adequately predicting magnetopause positions, with
311 the majority (> 70%) showing RMSE within 1 RE. Our model demonstrates superior accuracy, with



312 80% of its prediction errors falling below 1 R_E . Predicting the magnetopause under disturbed solar
313 wind conditions is more challenging, while the POS model shows improved performance in such
314 conditions, with 60% of predictions remaining within 1 R_E . Given the inherent asymmetry of the
315 magnetopause, we evaluated the models' performance in both the flank region ($|\varphi| \geq 60^\circ$) and the higher
316 latitude region ($|\theta| \geq 30^\circ$). The POS model consistently outperforms the others in both regions,
317 especially in the flank region. Notably, as a time-dependent three-dimensional model, the POS model
318 seldom produces poor predictions, with RMSE exceeding 3 R_E in only rare cases.



319

320 **Figure 4.** Distribution of models' RMSE in total(a) and in disturbed solar wind(b); (c) and (d) is the
321 prediction ability in higher latitude magnetopause ($|\theta| \geq 30^\circ$) and in magnetopause flank region ($|\varphi| \geq 60^\circ$)



322 **4.1 Time-dependent feature**

323 The models' prediction accuracy is listed in Table 3, it can be seen that all evaluated models exhibit
 324 remarkable predictive capabilities, with $\Delta < 1 R_E$, aligning closely with other statistical results found in
 325 the literature (Staples et al., 2020b). While it should be noted that the Δ values calculated for other
 326 models in this study may slightly differ from those reported in their original papers. This discrepancy
 327 arises due to our use of a significantly larger MCE dataset for comparison.

328 **Table 3 Models' prediction accuracy for all MCEs and in disturbed solar wind.**

Model Name	Total (38,887 MCEs)		[$\sigma(P_{dyn}) / \langle P_{dyn} \rangle > 100\%$] (1,048 MCEs)	
	$\Delta(R_E)$	$\delta(\Delta) / \Delta_{POS}$	$\Delta(R_E)$	$\delta(\Delta) / \Delta_{POS}$
PR96	0.899	+16.9%	1.389	+26.4%
S97	0.884	+15.0%	1.383	+25.8%
S98	0.894	+16.3%	1.388	+26.3%
C02	0.926	+20.4%	1.325	+20.6%
L10	0.960	+24.8%	1.377	+25.3%
POS	0.769	Average:18.7%	1.099	Average:24.9%

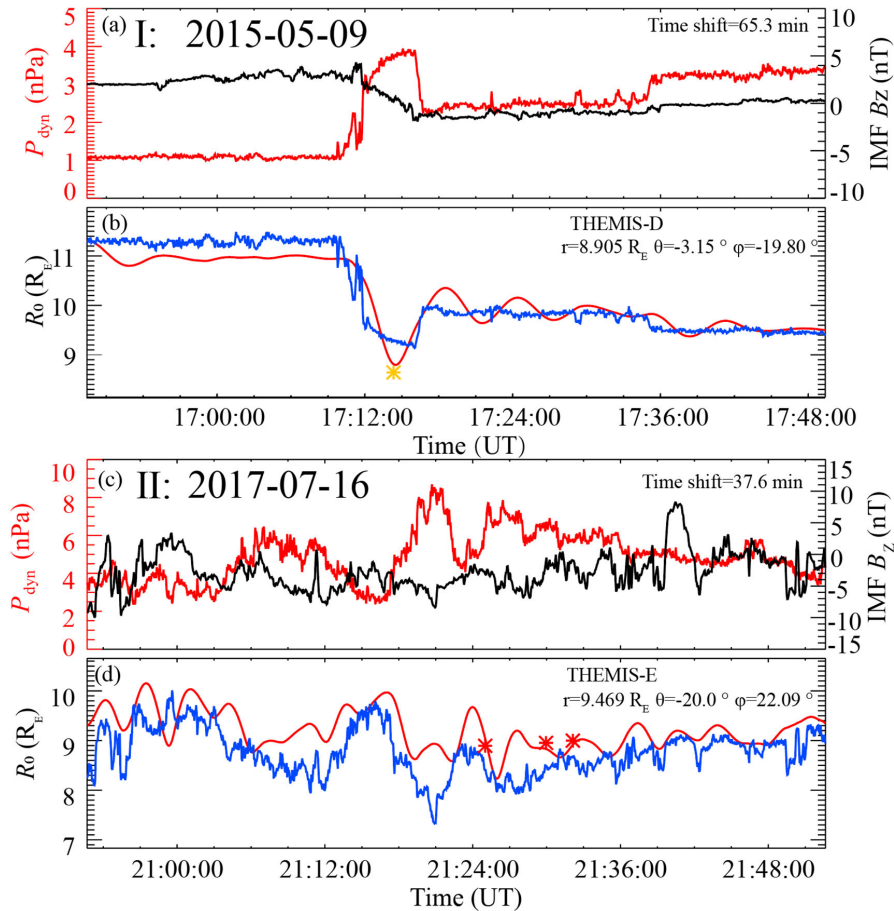
329 Notably, the POS model demonstrates superior predictive performance, with an average
 330 improvement of 18.7% over the other models. Additionally, time-independent models have inherent
 331 limitations in capturing the dynamic response of the magnetosphere to solar wind fluctuations,
 332 particularly when the magnetopause standoff distance is not in phase with P_{dyn} (Archer et al., 2019).
 333 In cases of highly disturbed upstream solar wind, where ratio of standard deviation of P_{dyn} to average
 334 P_{dyn} ($\sigma(P_{dyn}) / \langle P_{dyn} \rangle$) exceeding 100%, the POS model shows an even greater improvement in
 335 predictive accuracy, with a 24.9% enhancement compared to other models. These results suggest that
 336 by incorporating time-dependent effects into magnetopause modelling, particularly during periods of
 337 solar wind disturbance, the POS model can more effectively capture the non-linear and out-of-phase
 338 responses of the magnetopause to rapidly changing solar wind conditions. This results also indicate



339 that time-dependent model represents an obvious advancement in predicting and understanding
340 magnetospheric dynamics across a wide range of solar wind conditions.

341

342 The magnetopause is rarely static, exhibiting continuous motion under varying solar wind
343 conditions and displaying complex dynamics during both intense disturbances and gentle changes. A
344 notable feature of these dynamics is the periodic oscillation within the Pc5 frequency range (2-7 mHz),
345 often termed the “magic frequency” in magnetospheric physics (Samson et al., 1992; Plaschke et al.,
346 2009a; Plaschke et al., 2009b). The magnetopause oscillations can be driven by quasi-periodic solar
347 wind dynamic fluctuations, or explained by magnetospheric cavity mode and Kruskal-Schwarzschild
348 mode (Archer et al., 2013; Kruskal and Schwarzschild, 1954; Kepko and Spence, 2003; Kivelson et
349 al., 1984). Our previous research indicates that the oscillations of the magnetopause ought to have
350 eigenfrequencies (f_0) which are determined by the restoring force (P_B), the external driving force (P_{dyn})
351 as well as the damping force (P_{damp}) (David Halliday, 2021; Freeman et al., 1995; Gu et al.,
352 2023). Magnetopause will responses to solar wind with phase difference ranging from 0 to 180 degrees,
353 depending on the driving frequency of the solar wind (f_{drive}). The magnetopause behaves as a low-pass
354 filter, effectively screening out very high-frequency solar wind fluctuations (e.g., $f_{drive} > 15f_0$, where f_0
355 is the eigenfrequency of the magnetopause). This filtering effect results in smoother predictions of
356 magnetopause behaviour which could be found in Figure 5. For relatively high fluctuations (e.g., $15f_0 >$
357 $f_{drive} > 2f_0$), the phase difference between the solar wind and magnetopause approaches 180 degrees,
358 indicating an anti-phase response. At resonance ($f_{drive} \approx f_0$), the magnetopause exhibits a 90-degree
359 phase lag relative to the solar wind forcing. Conversely, the magnetopause only behaves in-phase with
360 the solar wind under low-frequency fluctuations ($f_{drive} < 0.5f_0$), which is the scenario typically revealed
361 by time-independent models.



362

363 **Figure 5. Case study for the overall oscillation of magnetopause using time-independent model S98 and**
 364 **time-dependent POS model to predict the its position. (a), (c) The corresponding upstream solar wind**
 365 **dynamic pressure P_{dyn} (red line) and interplanetary magnetic field B_z component (black line) observed by**
 366 **Wind with a time shift of 65.3 min and 37.6 min, respectively; (b), (d)The predictions of S98(blue) and POS**
 367 **(red) model's prediction based the input solar wind and the subsolar point position projected from**
 368 **THEMIS. The asterisks represent the positions of MCEs observed by THEMIS.**

369 The time-dependent POS model demonstrates the capability to depict these magnetosphere
 370 oscillations and the phase difference accurately. Figure 5 presents two specific cases illustrating the
 371 POS model's performance. In both cases, the model predicts quasi-periodic oscillations in the
 372 magnetopause that align well with consecutive THEMIS MCE observations. In Case I, both models



373 initially predict the magnetopause position at $\sim 11.5 R_E$ before a pressure pulse in solar wind. The POS
374 model uniquely predicts four oscillations around its equilibrium position ($\sim 10 R_E$) before the
375 magnetopause reaches a new pressure balance. This dynamic behaviour cannot be physically captured
376 by any time-independent models. In Case II, the POS model accurately captures the oscillations around
377 21:24 UT–21:33 UT, which are not all in-phase with the solar wind dynamic pressure (P_{dyn}). Notably,
378 the POS model depicts anti-phase responses observed in the second and third crossings, while the S98
379 model shows a reverse trend in motion that deviates more from observations. These results suggest
380 that by incorporating time-dependent effects into magnetopause modelling, particularly during periods
381 of solar wind disturbance, the POS model can more effectively capture the non-linear and out-of-phase
382 responses of the magnetopause to rapidly changing solar wind conditions.

383 **4.2 Three-dimensional characteristic**

384 The POS model developed here incorporates the asymmetrical effects of dipole tilt angles,
385 latitude, and longitude differences, as integrated into equations (2) and (3). The model's parameters
386 were comprehensively calibrated, allowing it to more accurately depict the three-dimensional shape of
387 the magnetopause. To assess its validity across different magnetopause regions, extensive tests were
388 performed, with results presented in Table 4. In the higher latitude magnetopause ($|\theta| \geq 30^\circ$), a region
389 where many models face challenges, the POS model, alongside the L10 model, demonstrates superior
390 performance, showing an impressive 28.7% improvement in accuracy compared to other models.
391 Similarly, in the flank regions ($|\phi| \geq 60^\circ$), where surface waves and other magnetospheric fluctuations
392 complicate position and shape determination, the POS model maintains its high accuracy, with a 35.2%
393 improvement over other models. These results suggest that the POS model offers a more accurate and
394 comprehensive representation of the magnetopause across its entire structure, outperforming other
395 models in both higher latitude and flank regions.

396

397



398

Table 4 Models' prediction accuracy for higher latitude and flank regions

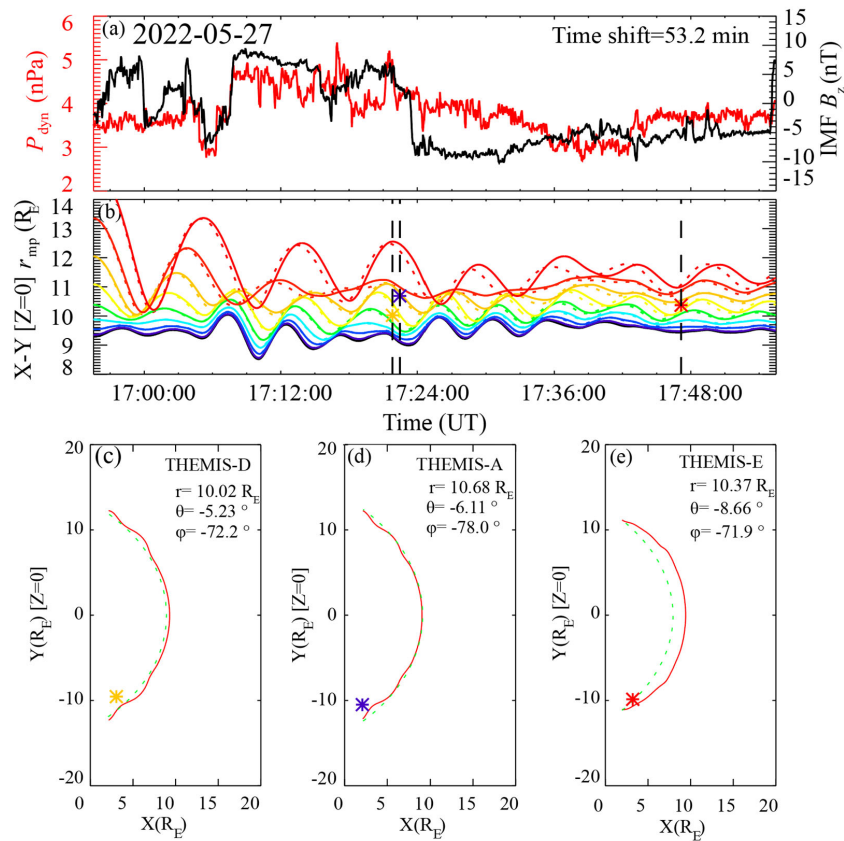
Model name	$ \theta \geq 30^\circ$ (7,325 MCEs)		$ \phi \geq 60^\circ$ (5,410 MCEs)	
	$\langle \Delta \rangle (R_E)$	$\delta (\Delta) / \Delta_{POS}$	$\Delta (R_E)$	$\delta (\Delta) / \Delta_{POS}$
PR96	1.149	+29.5%	1.315	+33.6%
S97	1.180	+33.0%	1.388	+41.1%
S98	1.195	+34.7%	1.403	+42.6%
C02	1.130	+27.4%	1.268	+28.9%
L10	1.053	+18.7%	1.278	+29.9%
POS	0.887	Average:28.7%	0.984	Average:35.2%

399

400 Surface waves are a distinct feature of the magnetopause, originating from various factors
 401 including solar wind and bow shock dynamics, as well as instabilities within the magnetopause and
 402 magnetosphere under specific conditions. Several localized physical processes have been identified as
 403 potential drivers of these surface waves, including the Kelvin-Helmholtz instability, magnetic
 404 reconnection and flux transfer event (Hartinger et al., 2013; Agapitov et al., 2009; Archer et al., 2021).
 405 It is also found tailward-moving surface wavelet could be driven by disturbed solar wind (large σ
 406 $(P_{dyn}) / \langle P_{dyn} \rangle$) (Sibeck et al., 1989). Our previous study has revealed a distinct mechanism for the
 407 formation of surface wave-like structures in the magnetopause (Gu et al., 2023). The interplay between
 408 dynamic pressure (P_{dyn}), magnetic pressure (P_b), and damping pressure (P_{damp}) results in different
 409 oscillation periods at various points on the magnetopause. These variations create a time lag within the
 410 magnetopause structure, manifesting as a surface wave-like pattern. Figure 6 shows a surface wave-
 411 like structure predicted by the POS model during relatively disturbed upstream solar wind conditions.
 412 The POS model's predictions are compared with those of the C02 model, which has been demonstrated
 413 as the most effective time-independent model in the flank region according to our evaluation. Figure
 414 6 (a) displays the solar wind dynamic pressure and the north-south component of the interplanetary
 415 magnetic field. The radial positions of various points on the magnetopause in the XY plane ($Z=0$), as



416 calculated by the POS model, are traced in Figure 6(b). Notably, the magnetopause shapes calculated
 417 in Figures 6(c)-(e) reveal surface wave-like structures evolving over time. THEMIS MCEs observed
 418 in the flank region corroborate this predicted surface wave-like structure, indicating that the
 419 magnetopause position predicted by the POS model is more accurate than that predicted by the C02
 420 model.



421

422 **Figure 6. A surface wave-like structure in X-Y magnetopause flank region. (a) The corresponding solar wind**
 423 **dynamic pressure (red) and IMF B_z component (black), (b) The red, orange, yellow, green, blue, purple and**
 424 **black colours represent the initial magnetopause positions at $\phi = \pm 80^\circ$, $\pm 70^\circ$, $\pm 60^\circ$, $\pm 50^\circ$, $\pm 40^\circ$, $\pm 30^\circ$,**
 425 **$\pm 20^\circ$, $\pm 10^\circ$, 0° , respectively (dot line is the corresponding negative value of ϕ). The asterisk in purple**
 426 **(THEMIS-A), yellow (THEMIS-D) and red (THEMIS-E) indicate the satellite observation of MCEs**



427 **projected onto the X-Y(Z=0) plane; (c) (d) (e) The shape of magnetopause in the X-Y plane at different time**
428 **predicted by POS model (red dash line) and C02 model (green dot line).**

429 The POS model's predictions are compared with those of the C02 model, which has been
430 demonstrated as the most effective time-independent model in the flank region according to our
431 evaluation. Figure 6 illustrates a surface wave-like structure predicted by the POS model during
432 relatively disturbed upstream solar wind conditions. The predicted surface wave-like structure is
433 corroborated by THEMIS MCEs in the flank region, where the actual magnetopause position is closer
434 to Earth than predicted by C02 model.

435 **5 Discussion and Conclusion**

436 Accurately calculating the position of the magnetopause is essential for space weather forecasting
437 and understanding the underlying physical mechanisms involved in the solar wind- magnetosphere
438 interaction. In this work, we developed the POS model, the first time-dependent three-dimensional
439 magnetopause model based on quasi-elastodynamic theory. By incorporating key solar wind
440 parameters such as P_{dyn} , IMF B_z and Φ , this model effectively depicts magnetopause dynamics. The
441 POS model offers a new approach to describing magnetopause position, overall oscillation, and surface
442 wave-like structures as interconnected phenomena. Its time-dependent feature excels in capturing
443 dynamic processes, particularly under highly disturbed solar wind conditions. The three-dimensional
444 nature allows for accurate depiction of the overall magnetopause shape, with notable precision in
445 higher latitude regions and flank areas. This capability addresses limitations in existing models and
446 provides a more comprehensive picture of magnetopause dynamics from a different perspective.
447 However, there are still limitations and areas for improvement that future research should address:

448 (1) Adapting to extreme solar wind conditions: Similar to the force-deformation relationship of a
449 spring that requires a specific range of applicability, the POS model has not been specifically optimized
450 for extreme solar wind conditions (e.g., $P_{\text{dyn}} < 0.5$ nPa and $P_{\text{dyn}} > 10$ nPa). When the solar wind dynamic
451 pressure is low, the quasi-elastic process between the solar wind and the magnetopause exhibits



452 stronger damping characteristics, while at very high solar wind dynamic pressures, the magnetopause
453 shows increased rigidity. Future iterations could incorporate more suitable damping coefficients and
454 include P_{dyn} in the magnetospheric compressibility coefficient to broaden the model's applicability
455 range.

456 (2) Incorporating additional solar wind factors: Existing research has shown that even under
457 similar solar wind dynamic pressure conditions, changes in solar wind density and velocity have
458 distinct effects on magnetopause position (Samsonov et al., 2020). Additionally, the influence of solar
459 wind temperature, more comprehensive IMF effects (e.g., B_x and B_y), and other solar wind components
460 (e.g., alpha particles) on magnetopause position are not reflected in the current model. Future models
461 could consider introducing these factors to achieve better predictive results.

462 (3) Better nightside extension: The current POS model is primarily based on the dayside quasi-
463 elastodynamic theory and is calibrated and validated using dayside MCEs. In the future, the model's
464 calculation results for the nightside region could be improved by combining the fitting approach of
465 empirical models with a more flexible curve function calibrated using a larger number of nightside
466 MCE observations.

467 (4) Cusp region representation: Accurately modelling the magnetopause cusp region, shaped by
468 Earth's dipole field, remains challenging. While some models approximate this region by fitting two
469 distinct curves, capturing its shape and position precisely is complex. Improving the representation of
470 the cusp region will require further analysis of higher latitude satellite data to enhance model accuracy.

471 (5) Parameter fine-tuning: Further refinement of model parameters, potentially through machine
472 learning techniques or implementing piecewise functions for different regions, could improve the
473 model's accuracy. However, as noted in the introduction, it's important to balance model complexity
474 with practicality. Overly complex parameter expressions can lead to increased inconvenience and



475 higher computational costs. For those seeking the highest possible prediction accuracy, a more
476 practical approach might involve using numerical simulations.

477 The upcoming SMILE mission (Solar wind Magnetosphere Ionosphere Link Explorer), a joint
478 mission between the Chinese Academy of Sciences and the European Space Agency, is set to launch
479 in 2025. This mission will provide more detailed data on magnetopause position and polar cap shape
480 over time, enhancing the ability to validate and refine existing magnetopause models.

481 In summary, this study introduces the POS model, the first time-dependent three-dimensional
482 magnetopause model based on quasi-elastodynamic theory. Unlike time-independent models, the POS
483 model effectively captures the dynamic movement of the magnetopause under varying solar wind
484 conditions. When compared to five widely used models, the POS model demonstrates superior
485 predictive accuracy, showing a 18.7% improvement with $RMSE=0.768 R_E$. As a time-dependent
486 model, it demonstrated superior accuracy under highly disturbed solar wind conditions (24.9% better).
487 Its three-dimensional nature allows for enhanced accuracy in higher latitude regions (28.7% better)
488 and flank regions (35.2% better) of the magnetopause. Moreover, compared to numerical simulations,
489 the POS model offers a concise formulation with rapid computational speed, making it feasible for
490 direct deployment on satellites in the future, where onboard chips could complete calculations, greatly
491 enhancing satellite intelligence. By providing a more precise and dynamic representation of the
492 magnetopause, the POS model enhances our ability to predict and analyse space weather events and
493 may also offer new insights and methodologies for developing magnetopause models for other planets.

494

495 **Code and data availability**

496 The current version of model is available from the project
497 website: http://www.spaceweather.org.cn/pos_model. The exact version of the model used to produce
498 the results used in this paper is archived on Zenodo: <https://doi.org/10.5281/zenodo.14189153>. The



499 URL includes the code and the list of MCEs used in this paper. The data of THEMIS satellite can be
500 obtained from <https://cdaweb.gsfc.nasa.gov/pub/data/themis/> , and the data of WIND satellite can be
501 obtained from <https://cdaweb.gsfc.nasa.gov/pub/data/wind/> .

502 **Competing interests**

503 The contact author has declared that none of the authors has any competing interests.

504 **Author contribution**

505 Y. W. designed the model. Y.X.G developed the model code and carried them out. Y. X. G and
506 Y. W. prepared the original manuscript. Y. X. G and X. J. S. prepared the MCE list. F. S. W., X. S. F.,
507 A. S., X. J. S., B. Y. W., P. B. Z., C. W. J., Y. L. C, X. J. X. and Z. L. Z. discussed the scientific results,
508 reviewed and revised the manuscript.

509 **Acknowledgements**

510 We thank NASA/GSFC CDAWeb for providing the Wind, THEMIS and Cluster data. This work
511 is jointly supported by the National Natural Science Foundation of China 42174199, China Scholarship
512 Council 202306120305, Guangdong Basic and Applied Basic Research Foundation
513 2023B1515040021, and Shenzhen Technology Project JCYJ20210324121210027 and
514 RCJC20210609104422048, and Shenzhen Key Laboratory Launching Project No.
515 ZDSYS20210702140800001.



References

- Agapitov, O., Glassmeier, K.-H., Plaschke, F., Auster, H.-U., Constantinescu, D., Angelopoulos, V., Magnes, W., Nakamura, R., Carlson, C. W., Frey, S., and McFadden, J. P.: Surface waves and field line resonances: A THEMIS case study, *Journal of Geophysical Research: Space Physics*, 114, A00C27, 10.1029/2008ja013553, 2009.
- 520 Ala-Lahti, M., Pulkkinen, T. I., Pfau-Kempf, Y., Grandin, M., and Palmroth, M.: Energy Flux Through the Magnetopause During Flux Transfer Events in Hybrid-Vlasov 2D Simulations, *Geophysical Research Letters*, 49, 10.1029/2022gl100079, 2022.
- Anderson, K. A., Binsack, J. H., and Fairfield, D. H.: HYDROMAGNETIC DISTURBANCES OF 3- TO 15-MINUTE PERIOD ON MAGNETOPOUSE AND THEIR RELATION TO BOW SHOCK SPIKES, *Journal of Geophysical Research*, 73, 2371-2386, 10.1029/JA073i007p02371, 1968.
- 525
- Angelopoulos, V.: The THEMIS mission, *Space Science Reviews*, 141, 5-34, 10.1007/s11214-008-9336-1, 2008.
- Archer, M. O., Hartinger, M. D., and Horbury, T. S.: Magnetospheric “magic” frequencies as magnetopause surface eigenmodes, 40, 5003-5008, <https://doi.org/10.1002/grl.50979>, 2013.
- Archer, M. O., Hartinger, M. D., Plaschke, F., Southwood, D. J., and Rastaetter, L.: Magnetopause ripples going against the flow form azimuthally stationary surface waves, *Nature Communications*, 12, 10.1038/s41467-021-25923-7, 2021.
- 530
- Archer, M. O., Hietala, H., Hartinger, M. D., Plaschke, F., and Angelopoulos, V.: Direct observations of a surface eigenmode of the dayside magnetopause, *Nature Communications*, 10, 10.1038/s41467-018-08134-5, 2019.
- Ashida, Y., Yamakawa, H., Funaki, I., Usui, H., Kajimura, Y., and Kojima, H.: Thrust Evaluation of Small-Scale Magnetic Sail Spacecraft by Three-Dimensional Particle-in-Cell Simulation, *Journal of Propulsion and Power*, 30, 186-196, 10.2514/1.B35026, 2014.
- 535
- Aubry, M. P., Russell, C. T., and Kivelson, M. G. J. o. G. R.: Inward motion of the magnetopause before a substorm, 75, 7018-7031, 1970.
- Auster, H. U., Glassmeier, K. H., Magnes, W., Aydogar, O., Baumjohann, W., Constantinescu, D., Fischer, D., Fornacon, K. H., Georgescu, E., Harvey, P., Hillenmaier, O., Kroth, R., Ludlam, M., Narita, Y., Nakamura, R., Okrafka, K., Plaschke, F., Richter, I., Schwarzl, H., Stoll, B., Valavanoglou, A., and Wiedemann, M.: The THEMIS Fluxgate Magnetometer, *Space Science Reviews*, 141, 235-264, 10.1007/s11214-008-9365-9, 2008.
- 540
- Balogh, A., Dunlop, M. W., Cowley, S. W. H., Southwood, D. J., Thomlinson, J. G., Glassmeier, K. H., Musmann, G., Lühr, H., Buchert, S., Acuña, M. H., Fairfield, D. H., Slavin, J. A., Riedler, W., Schwingenschuh, K., and Kivelson, M. G.: The Cluster Magnetic Field Investigation, in: *The Cluster and Phoenix Missions*, edited by: Escoubet, C. P., Russell, C. T., and Schmidt, R., Springer Netherlands, Dordrecht, 65-91, 10.1007/978-94-011-5666-0_3, 1997.
- 545
- Beard, D. B.: The interaction of the terrestrial magnetic field with the solar corpuscular radiation, 65, 3559-3568, <https://doi.org/10.1029/JZ065i011p03559>, 1960.
- Boardsen, S. A., Eastman, T. E., Sotirelis, T., and Green, J. L.: An empirical model of the high-latitude magnetopause, 105, 23193-23219, <https://doi.org/10.1029/1998JA000143>, 2000.
- 550
- Borovsky, J. E. and Alejandro Valdivia, J.: The Earth's Magnetosphere: A Systems Science Overview and Assessment, *Surveys in Geophysics*, 39, 817-859, 10.1007/s10712-018-9487-x, 2018.
- Børve, S., Sato, H., Pécseli, H., and Trulsén, J.: Minute-scale period oscillations of the magnetosphere, *Annales Geophysicae*, 29, 663-671, 10.5194/angeo-29-663-2011, 2011.
- Chao, J., Wu, D., Lin, C.-H., Yang, Y.-H., Wang, X., Kessel, M., Chen, S., and Lepping, R.: Models for the size and shape of the Earth's magnetopause and bow shock, *Cospar Colloquia series*, 127-135,
- 555
- Chapman, S. and Ferraro, V. C. A.: A New Theory of Magnetic Storms, *Journal of Geophysical Research*, 38, 79-96, 10.1038/126129a0, 1930.
- Chen, C. X. and Wolf, R. A.: Theory of thin-filament motion in Earth's magnetotail and its application to bursty bulk



- flows, *Journal of Geophysical Research-Space Physics*, 104, 14613-14626, 10.1029/1999ja900005, 1999.
- 560 Chen, Y.-W., Shue, J.-H., Zhong, J., and Shen, H.-W.: Anomalous Response of Mercury's Magnetosphere to Solar Wind Compression: Comparison to Earth, *The Astrophysical Journal*, 957, 26, 10.3847/1538-4357/acf655, 2023.
- Choe, J. Y. and Beard, D. B.: The compressed geomagnetic field as a function of dipole tilt, *Planetary and Space Science*, 22, 595-608, [https://doi.org/10.1016/0032-0633\(74\)90093-2](https://doi.org/10.1016/0032-0633(74)90093-2), 1974a.
- Choe, J. Y. and Beard, D. B.: The near earth magnetic field of the magnetotail current, *Planetary and Space Science*, 22, 609-615, [https://doi.org/10.1016/0032-0633\(74\)90094-4](https://doi.org/10.1016/0032-0633(74)90094-4), 1974b.
- David Halliday, R. R., Jearl Walker: *Fundamentals of Physics, Extended*, 12th Edition, in: *Fundamentals of Physics, Extended*, 12th Edition, Wiley, 456-458, 2021.
- Desai, R. T., Freeman, M. P., Eastwood, J. P., Eggington, J. W. B., Archer, M. O., Shprits, Y. Y., Meredith, N. P., Staples, F. A., Rae, I. J., Hietala, H., Mejnertsen, L., Chittenden, J. P., and Horne, R. B.: Interplanetary Shock-Induced Magnetopause Motion: Comparison Between Theory and Global Magnetohydrodynamic Simulations, *Geophysical Research Letters*, 48, 10.1029/2021gl092554, 2021.
- 570 Dungey, J. W.: Interplanetary Magnetic Field and the Auroral Zones, *Physical Review Letters*, 6, 47-48, 10.1103/PhysRevLett.6.47, 1961.
- Eastwood, J. P., Hietala, H., Toth, G., Phan, T. D., and Fujimoto, M.: What Controls the Structure and Dynamics of Earth's Magnetosphere?, *Space Science Reviews*, 188, 251-286, 10.1007/s11214-014-0050-x, 2015.
- 575 Escoubet, C. P., Fehringer, M., and Goldstein, M.: The Cluster mission - Introduction, *Annales Geophysicae*, 19, 1197-1200, 10.5194/angeo-19-1197-2001, 2001.
- Fairfield, D. H.: Average and unusual locations of the Earth's magnetopause and bow shock, 76, 6700-6716, <https://doi.org/10.1029/JA076i028p06700>, 1971.
- 580 Feng, X.: Current Status of MHD Simulations for Space Weather, in: *Magnetohydrodynamic Modeling of the Solar Corona and Heliosphere*, edited by: Feng, X., Springer Singapore, Singapore, 1-123, 10.1007/978-981-13-9081-4_1, 2020.
- Ferraro, V. C. A.: On the theory of the first phase of a geomagnetic storm: A new illustrative calculation based on an idealised (plane not cylindrical) model field distribution, 57, 15-49, <https://doi.org/10.1029/JZ057i001p00015>, 1952.
- Formisano, V., Domingo, V., and Wenzel, K.-P.: The three-dimensional shape of the magnetopause, *Planetary and Space Science*, 27, 1137-1149, 10.1016/0032-0633(79)90134-x, 1979.
- 585 Freeman, M. P. and Farrugia, C. J.: Magnetopause motions in a Newton-Busemann approach, *Nato Adv Sci I C-Mat*, 509, 15-26, 1998.
- Freeman, M. P., Freeman, N. C., and Farrugia, C. J.: A Linear Perturbation Analysis of Magnetopause Motion in the Newton-Busemann Limit, *Ann Geophys*, 13, 907-918, DOI 10.1007/s005850050230, 1995.
- 590 Gargaté, L., Fonseca, R. A., Bingham, R., and Silva, L. O.: Expansion of a plasma cloud into the solar wind, *Ieee Transactions on Plasma Science*, 36, 1168-1169, 10.1109/tps.2008.922424, 2008.
- Grimmich, N., Plaschke, F., Grison, B., Prencipe, F., Escoubet, C. P., Archer, M. O., ... Maggiolo, R.: Cluster Magnetopause Crossings between 2001 and 2020 [dataset], <https://doi.org/10.17605/OSF.IO/PXCTG>, 2024.
- Gu, Y. X., Wang, Y., Wei, F. S., Feng, X. S., Song, X. J., Wang, B. Y., Zuo, P. B., Jiang, C. W., Xu, X. J., and Zhou, Z. L.: Quasi-elastodynamic Processes Involved in the Interaction between Solar Wind and Magnetosphere, *The Astrophysical Journal*, 946, 102, 10.3847/1538-4357/acbe9b, 2023.
- 595 Haerendel, G.: Field-Aligned Currents in the Earth's Magnetosphere, in: *Physics of Magnetic Flux Ropes*, *Geophysical Monograph Series*, 539-553, <https://doi.org/10.1029/GM058p0539>, 1990.
- 600 Hartinger, M. D., Turner, D. L., Plaschke, F., Angelopoulos, V., and Singer, H.: The role of transient ion foreshock phenomena in driving Pc5 ULF wave activity, *Journal of Geophysical Research: Space Physics*, 118, 299-312,



- <https://doi.org/10.1029/2012JA018349>, 2013.
- Hu, Y.-Q., Guo, X.-C., Li, G.-Q., Wang, C., and Huang, Z.-H.: Oscillation of Quasi-Steady Earth's Magnetosphere, 22, 2723, 10.1088/0256-307x/22/10/073, 2005.
- 605 Kepko, L. and Spence, H. E.: Observations of discrete, global magnetospheric oscillations directly driven by solar wind density variations, *Journal of Geophysical Research-Space Physics*, 108, 10.1029/2002ja009676, 2003.
- Kivelson, M. G., Etcheto, J., and Trotignon, J. G.: Global compressional oscillations of the terrestrial magnetosphere: The evidence and a model, 89, 9851-9856, <https://doi.org/10.1029/JA089iA11p09851>, 1984.
- Kruskal, M. and Schwarzschild, M.: SOME INSTABILITIES OF A COMPLETELY IONIZED PLASMA, *Proceedings of the Royal Society of London Series a-Mathematical and Physical Sciences*, 223, 348-360, 10.1098/rspa.1954.0120, 1954.
- 610 Lepping, R. P., Acuña, M. H., Burlaga, L. F., Farrell, W. M., Slavin, J. A., Schatten, K. H., Mariani, F., Ness, N. F., Neubauer, F. M., Whang, Y. C., Byrnes, J. B., Kennon, R. S., Panetta, P. V., Scheifele, J., and Worley, E. M.: The WIND magnetic field investigation, *Space Science Reviews*, 71, 207-229, 10.1007/BF00751330, 1995.
- Lin, R., Anderson, K., Ashford, S., Carlson, C., Curtis, D., Ergun, R., Larson, D., McFadden, J., McCarthy, M., and Parks, G. J. S. S. R.: A three-dimensional plasma and energetic particle investigation for the Wind spacecraft, 71, 125-153, 1995.
- 615 Lin, R. L., Zhang, X. X., Liu, S. Q., Wang, Y. L., and Gong, J. C.: A three-dimensional asymmetric magnetopause model, 115, <https://doi.org/10.1029/2009JA014235>, 2010.
- Lyon, J. G., Fedder, J. A., and Mobarry, C. M.: The Lyon-Fedder-Mobarry (LFM) global MHD magnetospheric simulation code, *Journal of Atmospheric and Solar-Terrestrial Physics*, 66, 1333-1350, 10.1016/j.jastp.2004.03.020, 2004.
- 620 Mann, I. R., Murphy, K. R., Ozeke, L. G., Rae, I. J., Milling, D. K., Kale, A. A., and Honary, F. F.: The Role of Ultralow Frequency Waves in Radiation Belt Dynamics, in: *Dynamics of the Earth's Radiation Belts and Inner Magnetosphere*, 69-92, <https://doi.org/10.1029/2012GM001349>, 2012.
- Matsuoka, H., Takahashi, K., and Yumoto, K.: Observation and modeling of compressional Pi 3 magnetic pulsations, 100, 10.1029/94JA03368, 1995.
- 625 McFadden, J., Carlson, C., Larson, D., Ludlam, M., Abiad, R., Elliott, B., Turin, P., Marckwordt, M., and Angelopoulos, V.: The THEMIS ESA plasma instrument and in-flight calibration, *Space Science Reviews*, 141, 277-302, 10.1007/s11214-008-9440-2, 2008.
- Mead, G. D. and Beard, D. B.: Shape of the geomagnetic field solar wind boundary, *Journal of Geophysical Research*, 69, 1169-1179, 10.1029/jz069i007p01169, 1964.
- 630 Merkin, V. G. and Lyon, J. G.: Effects of the low-latitude ionospheric boundary condition on the global magnetosphere, *Journal of Geophysical Research: Space Physics*, 115, <https://doi.org/10.1029/2010JA015461>, 2010.
- Moritaka, T., Kajimura, Y., Usui, H., Matsumoto, M., Matsui, T., and Shinohara, I.: Momentum transfer of solar wind plasma in a kinetic scale magnetosphere, *Physics of Plasmas*, 19, 10.1063/1.3683560, 2012.
- Mottez, F.: Relationship between Alfvén Wave and Quasi-Static Acceleration in Earth's Auroral Zone, in: *Low-Frequency Waves in Space Plasmas*, 121-138, <https://doi.org/10.1002/9781119055006.ch8>, 2016.
- 635 Olson, W. P.: The shape of the tilted magnetopause, 74, 5642-5651, <https://doi.org/10.1029/JA074i024p05642>, 1969.
- Omelchenko, Y. A., Roytershteyn, V., Chen, L. J., Ng, J., and Hietala, H.: HYPERS simulations of solar wind interactions with the Earth's magnetosphere and the Moon, *Journal of Atmospheric and Solar-Terrestrial Physics*, 215, 10.1016/j.jastp.2021.105581, 2021.
- 640 P. Song, B. U. d. S., and M. F. Thomsen, Eds. : *Physics of the Magnetopause*, 5260, 364-364 pp., doi:10.1126/science.272.5260.364.a, 1996.
- Petrinec, S. M.: Nowcasting and Forecasting the Magnetopause and Bow Shock Locations Based on Empirical Models and Real-Time Solar Wind Data, in: *Space Weather*, 257-263, <https://doi.org/10.1029/GM125p0257>, 2001.



- Petrinec, S. M. and Russell, C. T.: Near-Earth magnetotail shape and size as determined from the magnetopause flaring angle, 101, 137-152, <https://doi.org/10.1029/95JA02834>, 1996.
- 645 Plaschke, F.: ULF Waves at the Magnetopause, in: Low-Frequency Waves in Space Plasmas, 193-212, <https://doi.org/10.1002/9781119055006.ch12>, 2016.
- Plaschke, F., Glassmeier, K. H., Sibeck, D. G., Auster, H. U., Constantinescu, O. D., Angelopoulos, V., and Magnes, W.: Magnetopause surface oscillation frequencies at different solar wind conditions, *Annales Geophysicae*, 27, 4521-4532, 10.5194/angeo-27-4521-2009, 2009a.
- 650 Plaschke, F., Glassmeier, K.-H., Auster, H. U., Constantinescu, O. D., Magnes, W., Angelopoulos, V., Sibeck, D. G., and McFadden, J. P.: Standing Alfvén waves at the magnetopause, 36, <https://doi.org/10.1029/2008GL036411>, 2009b.
- Powell, K. G., Roe, P. L., Linde, T. J., Gombosi, T. I., and De Zeeuw, D. L.: A solution-adaptive upwind scheme for ideal magnetohydrodynamics, *Journal of Computational Physics*, 154, 284-309, 10.1006/jcph.1999.6299, 1999.
- 655 Raeder, J., McPherron, R. L., Frank, L. A., Kokubun, S., Lu, G., Mukai, T., Paterson, W. R., Sigwarth, J. B., Singer, H. J., and Slavin, J. A.: Global simulation of the Geospace Environment Modeling substorm challenge event, *Journal of Geophysical Research: Space Physics*, 106, 381-395, <https://doi.org/10.1029/2000JA000605>, 2001.
- RÈMe, H., Bosqued, J. M., Sauvaud, J. A., Cros, A., Dandouras, J., Aoustin, C., Bouyssou, J., Camus, T., Cuvilo, J., Martz, C., MÉDale, J. L., Perrier, H., Romefort, D., Rouzaud, J., D'Uston, C., MÖBius, E., Crocker, K., Granoff, M., Kistler, L. M., Popecki, M., Hovestadt, D., Klecker, B., Paschmann, G., Scholer, M., Carlson, C. W., Curtis, D. W., Lin, R. P., McFadden, J. P., Formisano, V., Amata, E., Bavassano-Cattaneo, M. B., Baldetti, P., Belluci, G., Bruno, R., Chionchio, G., Di Lellis, A., Shelley, E. G., Ghielmetti, A. G., Lennartsson, W., Korth, A., Rosenbauer, H., Lundin, R., Olsen, S., Parks, G. K., McCarthy, M., and Balsiger, H.: THE CLUSTER ION SPECTROMETRY (CIS) EXPERIMENT, *Space Science Reviews*, 79, 303-350, 10.1023/A:1004929816409, 1997.
- 665 Russell, C. T.: The structure of the magnetopause, *Planetary and Space Science*, 51, 731-744, 10.1016/s0032-0633(03)00110-7, 2003.
- Samson, J. C., Harrold, B. G., Ruohoniemi, J. M., Greenwald, R. A., and Walker, A. D. M.: FIELD LINE RESONANCES ASSOCIATED WITH MHD WAVE-GUIDES IN THE MAGNETOSPHERE, *Geophysical Research Letters*, 19, 441-444, 10.1029/92gl00116, 1992.
- 670 Samsonov, A. A., Bogdanova, Y. V., Branduardi-Raymont, G., Sibeck, D. G., and Toth, G.: Is the Relation Between the Solar Wind Dynamic Pressure and the Magnetopause Standoff Distance so Straightforward?, *Geophysical Research Letters*, 47, e2019GL086474, <https://doi.org/10.1029/2019GL086474>, 2020.
- Samsonov, A. A., Gordeev, E., Tsyganenko, N. A., Šafránková, J., Němeček, Z., Šimůnek, J., Sibeck, D. G., Tóth, G., Merkin, V. G., and Raeder, J.: Do we know the actual magnetopause position for typical solar wind conditions?, *Journal of Geophysical Research: Space Physics*, 121, 6493-6508, <https://doi.org/10.1002/2016JA022471>, 2016.
- 675 Schield, M. A.: Pressure balance between solar wind and magnetosphere, 74, 1275-1286, <https://doi.org/10.1029/JA074i005p01275>, 1969.
- Shue, J.-H., Song, P., Russell, C. T., Steinberg, J. T., Chao, J. K., Zastenker, G., Vaisberg, O. L., Kokubun, S., Singer, H. J., Detman, T. R., and Kawano, H.: Magnetopause location under extreme solar wind conditions, 103, 17691-17700, <https://doi.org/10.1029/98JA01103>, 1998.
- 680 Shue, J. H., Chao, J. K., Fu, H. C., Russell, C. T., Song, P., Khurana, K. K., and Singer, H. J.: A New Functional form to Study the Solar Wind Control of the Magnetopause Size and Shape, *Journal of Geophysical Research*, 102, 9497, 10.1029/97ja00196, 1997.
- Shue, J. H., Chen, Y. S., Hsieh, W. C., Nowada, M., Lee, B. S., Song, P., Russell, C. T., Angelopoulos, V., Glassmeier, K. H., McFadden, J. P., and Larson, D.: Uneven compression levels of Earth's magnetic fields by shocked solar wind, *Journal of Geophysical Research: Space Physics*, 116, n/a-n/a, 10.1029/2010ja016149, 2011.
- 685 Sibeck, D. G.: The Magnetospheric and Ionospheric Response to Solar Wind Dynamic Pressure Variations, in: Modeling Magnetospheric Plasma Processes, 1-8, <https://doi.org/10.1029/GM062p0001>, 1991.



- 690 Sibeck, D. G., Baumjohann, W., Elphic, R. C., Fairfield, D. H., Fennell, J. F., Gail, W. B., Lanzerotti, L. J., Lopez, R. E., Luehr, H., Lui, A. T. Y., MacLennan, C. G., McEntire, R. W., Potemra, T. A., Rosenberg, T. J., and Takahashi, K.: The Magnetospheric Response to 8-Minute Period Strong-Amplitude Upstream Pressure Variations, *Journal of Geophysical Research-Space Physics*, 94, 2505-2519, 10.1029/JA094iA03p02505, 1989.
- Smit, G. R.: Oscillatory motion of the nose region of the magnetopause, 73, 4990-4993, <https://doi.org/10.1029/JA073i015p04990>, 1968.
- 695 Song, P., Elphic, R. C., and Russell, C. T.: ISEE-1 AND ISEE-2 OBSERVATIONS OF THE OSCILLATING MAGNETOPAUSE, *Geophysical Research Letters*, 15, 744-747, 10.1029/GL015i008p00744, 1988.
- Song, X., Zuo, P., and Zhou, Z.: Automatic Identification of Magnetopause Crossing Events, *Chinese Journal of Space Science*, 41, 375-383, 10.3724/SP.J.0254-6124.2021.0303, 2021.
- Spreiter, J. R., Summers, A. L., and Alksne, A. Y.: Hydromagnetic flow around the magnetosphere, *Planetary and Space Science*, 14, 223-253, [https://doi.org/10.1016/0032-0633\(66\)90124-3](https://doi.org/10.1016/0032-0633(66)90124-3), 1966.
- 700 Staples, F. A., Ashley, R. A., Forsyth, S. C., Jonathan, I., and Rae: THEMIS Magnetopause Crossing Database (1) [dataset], 10.5281/zenodo.3700504, 2020a.
- 705 Staples, F. A., Rae, I. J., Forsyth, C., Smith, A. R. A., Murphy, K. R., Raymer, K. M., Plaschke, F., Case, N. A., Rodger, C. J., Wild, J. A., Milan, S. E., and Imber, S. M.: Do Statistical Models Capture the Dynamics of the Magnetopause During Sudden Magnetospheric Compressions?, *Journal of Geophysical Research: Space Physics*, 125, e2019JA027289, 10.1029/2019ja027289, 2020b.
- Tóth, G., Sokolov, I. V., Gombosi, T. I., Chesney, D. R., Clauer, C. R., De Zeeuw, D. L., Hansen, K. C., Kane, K. J., Manchester, W. B., Oehmke, R. C., Powell, K. G., Ridley, A. J., Roussev, I. I., Stout, Q. F., Volberg, O., Wolf, R. A., Sazykin, S., Chan, A., Yu, B., and Kóta, J.: Space Weather Modeling Framework: A new tool for the space science community, *Journal of Geophysical Research: Space Physics*, 110, <https://doi.org/10.1029/2005JA011126>, 2005.
- 710 Tsyganenko, N. A.: A magnetospheric magnetic field model with a warped tail current sheet, *Planetary and Space Science*, 37, 5-20, [https://doi.org/10.1016/0032-0633\(89\)90066-4](https://doi.org/10.1016/0032-0633(89)90066-4), 1989.
- Tsyganenko, N. A.: Effects of the Solar Wind Conditions in the Global Magnetospheric Configurations as Deduced from Data-Based Field Models (Invited), *International Conference on Substorms*, October 01, 1996, 181,
- 715 Walker, R. J., Lapenta, G., Berchem, J., El-Alaoui, M., and Schriver, D.: Embedding particle-in-cell simulations in global magnetohydrodynamic simulations of the magnetosphere, *Journal of Plasma Physics*, 85, 10.1017/s0022377819000072, 2019.
- Wang, Y. and Chen, C. X.: Numerical Simulation of Radial Plasma Transport in the Saturn's Magnetosphere, *Chinese Journal of Geophysics*, 51, 635-642, 10.1002/cjg2.1235, 2008.
- Willis, D. M.: Structure of the magnetopause, 9, 953-985, <https://doi.org/10.1029/RG009i004p00953>, 1971.
- 720 Zong, Q., Escoubet, P., Sibeck, D., Le, G., and Zhang, H.: Dayside Magnetosphere Interactions, in: *Dayside Magnetosphere Interactions*, 303-306, <https://doi.org/10.1002/9781119509592.ch17>, 2020.